Annals of Biomedical Engineering
https://doi.org/10.1007/s10439-023-03426-4

BMES BIOMEDICAL ENGINEERING SOCIETY

ORIGINAL ARTICLE

Effect of Blood Pressure Levels on Sinus Hemodynamics in Relation to Calcification After Bioprosthetic Aortic Valve Replacement

Brennan Vogl[1] · Agata Sularz[2] · Scott Lilly[3] · Vinod H. Thourani[4] · Brian R. Lindman[5] · Mohamad Alkhouli[2] · Hoda Hatoum[1,6]

Received: 29 August 2023 / Accepted: 11 December 2023

Abstract

Coexisting hypertension and aortic stenosis are common. Some studies showed that elevated blood pressures may be associated with progression of calcific aortic valve disease (CAVD) while others showed no correlation. Flow dynamics in the sinuses of Valsalva are considered key factors in the progression of CAVD. While the relationship between hemodynamics and CAVD is not yet fully understood, it has been demonstrated that they are tightly correlated. This study aims to investigate the effect of changing systolic and diastolic blood pressures (SBP and DBP, respectively) on sinus hemodynamics in relation to potential initiation or progression of CAVD after aortic valve replacement (AVR). Evolut R, SAPIEN 3 and Magna valves were deployed in an aortic root under pulsatile conditions. Using particle image velocimetry, the hemodynamics in the sinus were assessed. The velocity, vorticity, circulation (Γ) and shear stress were calculated. This study shows that under elevated SBP and DBP, velocity, vorticity, and shear stress nearby the leaflets increased. Additionally, larger fluctuations of Γ and area under the curve throughout the cardiac cycle were observed. Elevated blood pressures are associated with higher velocity, vorticity, and shear stress near the leaflets which may initiate or accelerate pro-calcific changes in the prosthetic leaflets leading to bioprosthetic valve degeneration.

Keywords Hypertension · Particle image velocimetry · Sinus flow · Transcatheter aortic valve replacement · Surgical aortic valve replacement

Associate Editor Lakshmi Prasad Dasi oversaw the review of this article.

✉ Hoda Hatoum
hhatoum@mtu.edu

1 Biomedical Engineering Department, Michigan Technological University, 1400 Townsend Dr, Houghton, MI 49931, USA

2 Department of Cardiovascular Medicine, Mayo Clinic, Rochester, MN, USA

3 Department of Cardiovascular Medicine, The Ohio State University, Columbus, OH, USA

4 Department of Cardiovascular Surgery, Marcus Valve Center, Piedmont Heart Institute, Atlanta, GA, USA

5 Division of Cardiovascular Medicine, Structural Heart and Valve Center, Vanderbilt University Medical Center, Nashville, TN, USA

6 Health Research Institute, Center of Biocomputing and Digital Health and Institute of Computing and Cybernetics, Michigan Technological University, Houghton, MI, USA

Introduction

Calcific aortic valve disease (CAVD) is the most common heart valve disease in the United States with an increasing burden in the aging population [1]. In CAVD, calcium builds up on and within the valve leaflets, leading to stiffening. As stiffening progresses (aortic sclerosis to aortic stenosis), the valve opening becomes narrower leading to flow obstruction, elevated transvalvular pressure gradients and elevated pressure load on the ventricle [2]. Left untreated, aortic stenosis (AS) culminates in heart failure or sudden cardiac death [2].

Bioprosthetic aortic valve replacement (AVR)—transcatheter or surgical (TAVR, SAVR, respectively)—is the most effective and widely used therapeutic procedure to address AS [3]. One of the main drawbacks of bioprosthetic aortic valves is their durability and their susceptibility to structural valve degeneration (SVD) which can be initiated by calcification [4, 5]. Bioprosthetic aortic valves are composed of chemically stabilized animal tissues (xenografts) that offer better hemodynamic properties compared to their

Published online: 29 December 2023

mechanical alternatives, but their lifespan is shorter due to SVD [4, 5]. Glutaraldehyde can cause cell death on prostheses which inhibits their ability to pump calcium out of the cells leading to accumulation [6]. SVD can be initiated by structural changes to the prosthesis and leaflet calcification which ultimately affect hemodynamics.

Coexisting hypertension and AS are common, and studies have demonstrated that elevated blood pressures are associated with progression of valve calcification and stenosis [7–9]. However, other large prospective studies have not substantiated such a correlation [10]. Some studies showed that patients with hypertension and AS showed earlier symptoms [11]. It has been shown that the implantation of a bioprosthetic aortic valve leads to changes in the overall hemodynamics in the sinuses, the coronaries, and the arterial tree downstream of the aortic valve [12–18]. Immediately after AVR, blood pressure levels were found to increase, often necessitating treatment [19]. Optimum strategies for blood pressure moderation after AVR remain to be established, as low blood pressures have been associated with increased mortality [20–22]. Despite these relationships between blood pressure and aortic valve function, the effect of blood pressure on prosthetic valve durability has not been investigated.

From a fluid dynamic perspective, fluid shear stress is one of the major regulators of CAVD [2, 23] and flow dynamics in the sinuses of Valsalva are considered key factors in its progression [24, 25]. While the relationship between hemodynamics and CAVD is not yet fully understood, it has been demonstrated that they are tightly correlated [26]. CAVD limits the aortic valve opening, leading to changes on the sinus vortices and jet velocities. Non-physiological levels of viscous shear stress in the sinuses near the valve leaflets has been linked with CAVD [12–16, 23, 25, 27]. Non-physiological low shear stresses are associated with flow stasis and non-physiological elevated shear stresses are associated with hemostatic abnormalities [28].

In this study, we aim to investigate the effect of changing systolic and diastolic blood pressures (SBP, DBP, respectively) on sinus hemodynamics.

Methods

Hemodynamic Assessment

A 26 mm SAPIEN 3 balloon-expandable transcatheter heart valve (THV) (Edwards Lifesciences, Irvine, CA, USA), 29 mm Evolut R self-expanding THV (Minneapolis, MN, USA), and 25 mm Magna Ease surgical aortic valve (SAV) prosthesis (Edwards Lifesciences, Irvine, CA, USA) were implanted in an aortic root model within a pulse duplicating left heart simulator (Fig. 1) [18, 22, 29]. The

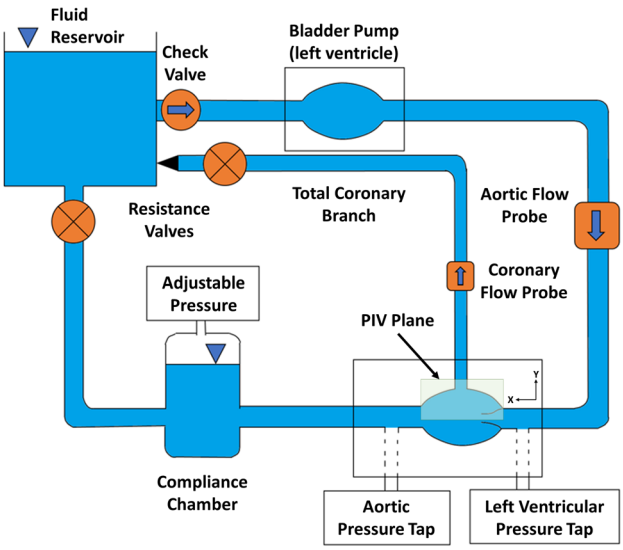

Fig. 1 Pulse duplicating left heart flow loop simulator setup with total coronary branch

flow loop was composed of a reservoir where the blood analog is stored, a mitral valve at the exit of the reservoir, a custom-made bladder pump that represents the ventricle, a flow probe (Transonic, NY, USA) that is connected to the flowmeter for average flow rate (cardiac output) measurement, aortic root chamber, compliance chamber to emulate arterial distensibility, and a gate resistance valve to control the cardiac output. The coronary loop was represented by a connection from the sinus to the storage reservoir with a pinch resistance valve to control the flow. This connection represented the total coronary flow, which was calculated to be 4–5% of the cardiac output (average minimum 200 ml/min and average maximum 250 ml/min). The average coronary flow was set within these physiological limits at 120/60 mmHg, by setting the resistance of the coronary circuit, at the beginning of the experiment. Then, once the baseline coronary conditions have been achieved, the coronary circuit parameters were held fixed as the systemic blood pressures were varied to evaluate the sole impact of aortic blood pressure on the resulting coronary flow. The blood analog selected was a mixture of water and glycerin (60–40% in volume) with a density of 1060 kg/m^3 and viscosity of 3.5 cP. The contraction and expansion of the bladder pump were controlled by an in-house developed LabVIEW (National Instruments, TX, USA) program. The experiments were performed at a cardiac output of 5L/min under a heart rate of 60 bpm and a range of SBP (100, 120, and 160 mmHg) and DBP (40, 60 and 90 mmHg). Pressures were measured using Millar catheters (ADinstruments, CO, USA) at the ventricular and aortic sides. Fifty consecutive cardiac cycles of pressure and flow rate data were recorded at a sampling rate of 100 Hz.

Particle Image Velocimetry (PIV)

PIV was performed to evaluate the flow dynamics within the sinus under different blood pressure conditions. The blood analog fluid, that is transparent, was seeded with rhodamine B particles of average size 10 µm. The sinus region was illuminated using a laser sheet created by pulsed Nd:YLF single cavity diode pumped solid state laser coupled with external spherical and cylindrical lenses while acquiring high-speed images of the fluorescent particles' displacement and movement within the sinus region. Time-resolved PIV images were acquired at a temporal resolution of 4000 Hz. Refraction was corrected using a calibration in DaVis particle image velocimetry software (DaVis 10, LaVision Germany). Velocity vectors were calculated in DaVis using advanced PIV cross-correlation approaches with a 50% overlap multipass approach starting from one 32 × 32-pixel interrogation followed by two 16 × 16-pixel interrogation passes. Post processing was performed using adaptive median filtering. This was performed similar to other published works by our team [12–16, 23, 25].

Using the velocity measurements, the out-of-plane vorticity (ω)—the curl of the velocity—was computed using Eq. (2) below:

$$\omega_z = -\left(\frac{\mathrm{d}V_x}{\mathrm{d}y} - \frac{\mathrm{d}V_y}{\mathrm{d}x}\right) \tag{1}$$

where ω_z is the vorticity component in s^{-1}, V_x and V_y are the x and y components of the velocity vector in m/s. The x and y directions are axial and lateral respectively with the z direction being out of measurement plane. The vorticity captures the rotational components of blood flow shearing and measures the tendency of the fluid to swirl [30].

Wall shear stress (τ) was computed as follows:

$$\tau = \mu\left(\frac{\mathrm{d}V_x}{\mathrm{d}y} + \frac{\mathrm{d}V_y}{\mathrm{d}x}\right) \tag{2}$$

where τ is the shear stress in Pa and μ is the dynamic viscosity in Pa s.

The circulation (Γ) was computed as follows within the sinus region:

$$\Gamma = \oint \vec{V}.\mathrm{d}\vec{l} = \int_S \vec{\omega}.\mathrm{d}\vec{S} \tag{3}$$

where Γ is the circulation (m^2/s), and $\vec{V}$ and $\vec{\omega}$ are the velocity and vorticity, respectively. Circulation is a macroscopic measure of rotation in an area of interest, that is the sinus in our case.

Results

Velocity and Vorticity in the Sinus

The increase in blood pressure, whether SBP or DBP, did not change the flow structures' presence in the sinus, such as the main sinus vortex or the secondary vortices. As the leaflets opened, the jet's velocity increased and at the edge of the leaflet the shear layers separated and were forced to curl into the sinus, leading to the emergence of the main sinus vortex at peak systole. The change in pressures, however, led to a change in the magnitudes of the velocity and vorticity.

Increasing SBP

Evolut R: Fig. 2 shows the velocity vectors and vorticity contours in the sinus and partially in the coronary artery with the Evolut R TAV at 60 bpm. Video 1 shows an example cardiac cycle. As SBP increased from 100 to 160 mmHg, the average velocity in the sinus increased from 0.0728 to 0.126 m/s, and more elevated vorticity magnitudes were noted with larger regions and with both clockwise (CW; blue contour) and counterclockwise (CCW; red contour) directions at peak systole. The increase in magnitude of the velocity in the sinus was also during acceleration, deceleration, and diastole, most notably during peak systole, deceleration, and diastole.

SAPIEN 3: Fig. 3 shows the velocity vectors and vorticity contours in the sinus and partially in the coronary artery with the SAPIEN 3 TAV at 60 bpm. Video 2 shows an example cardiac cycle. Like Evolut, the average velocity in the sinus increased from 0.0545 to 0.127 m/s as SBP increased from 100 to 160 mmHg. CW vorticity was prevalent in the sinus as the SBP increased. In the deceleration phase, more expanded vorticity regions were found as SBP increased and a change in the direction of the small vortices was noted going from CW to CCW.

Magna: Fig. 4 shows the velocity vectors and vorticity contours in the sinus and partially in the coronary artery with the Magna SAV at 60 bpm. Video 3 shows an example cardiac cycle. Like the Evolut R and SAPIEN 3, the average velocity in the sinus increased from 0.0471 to 0.0629 m/s. The difference in average velocity, however, was not as substantial in comparison. More expanded elevated vorticity zones were noted in the sinus with increasing SBP.

Increasing DBP

Evolut R: Fig. 5 shows the velocity vectors and vorticity contours in the sinus and partially in the coronary artery with the Evolut R TAV at 60 bpm. As DBP increased from

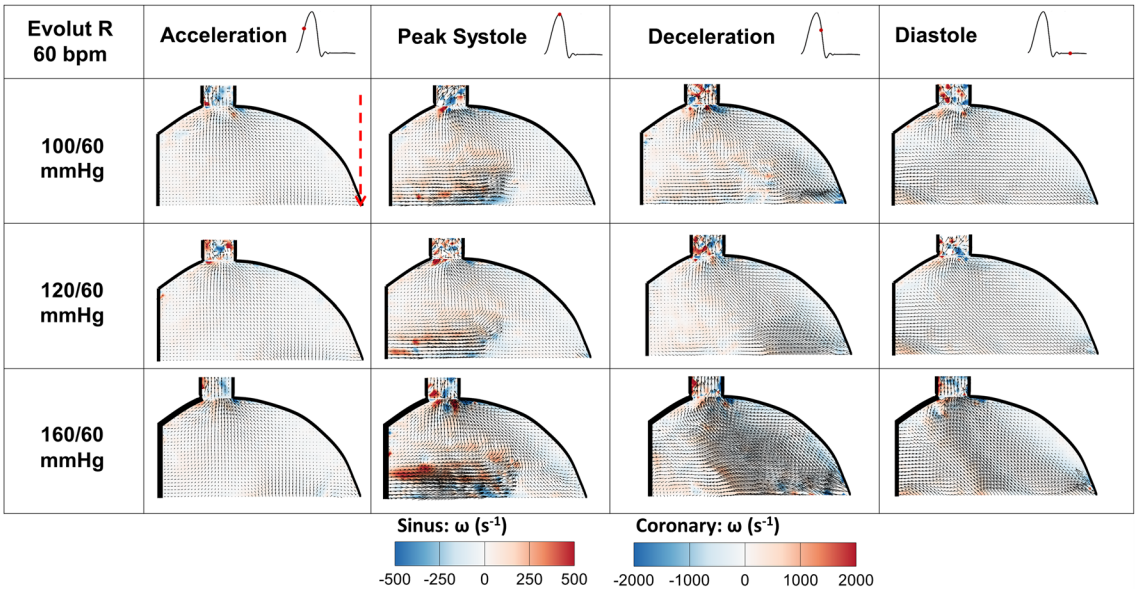

Fig. 2 Velocity vectors and vorticity contours in the sinus with increasing SBP in the presence of Evolut R. The dashed red arrow represents the location of the leaflet tip

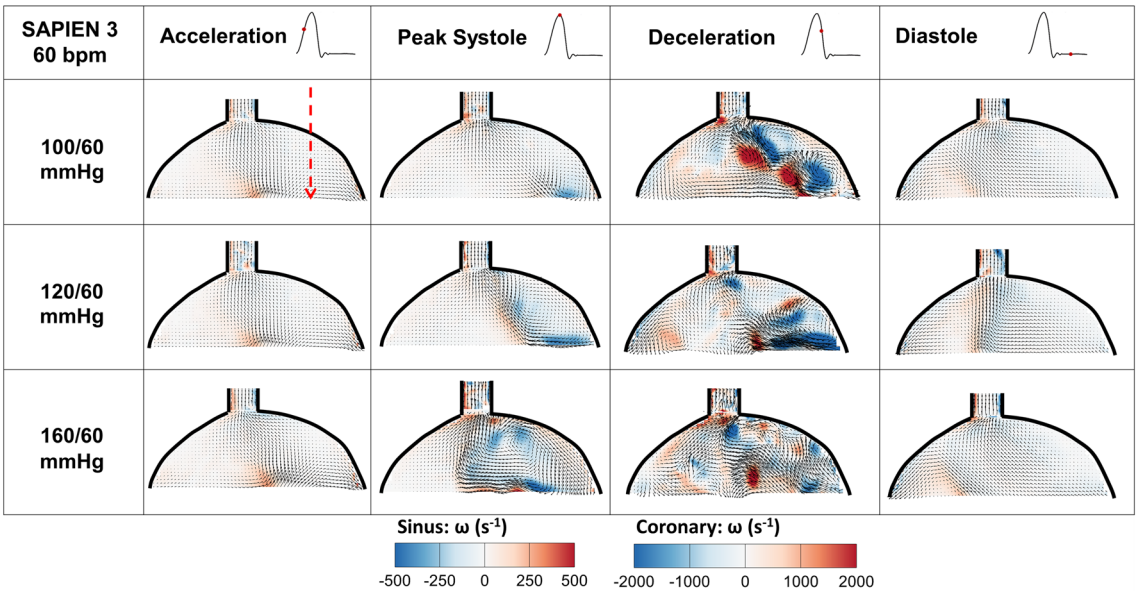

Fig. 3 Velocity vectors and vorticity contours in the sinus with increasing SBP in the presence of SAPIEN 3. The dashed red arrow represents the location of the leaflet tip

40 to 90 mmHg, the average velocity in the sinus increased from 0.0739 to 0.101 m/s. A slight difference in the distribution and magnitude of the vorticity is noticed as DBP increased. During deceleration, as DBP increased, the average sinus velocity decreased from 0.102 to 0.0695 m/s.

SAPIEN 3: Fig. 6 shows the velocity vectors and vorticity contours in the sinus and partially in the coronary artery with the SAPIEN 3 TAV at 60 bpm. The average velocity in the sinus stayed approximately constant as DBP increased from 40 to 90 mmHg to reach 0.0698 m/s at peak systole. The vorticity magnitude increased as DBP increased, only no change in the direction or distribution was noted at peak systole. During deceleration, as DBP increased, the average sinus velocity decreased from 0.23 to 0.131 m/s.

Magna: Fig 7 shows the velocity vectors and vorticity contours in the sinus and partially in the coronary artery with the Magna SAV at 60 bpm. At peak systole, the average velocity in the sinus increased from 0.0667

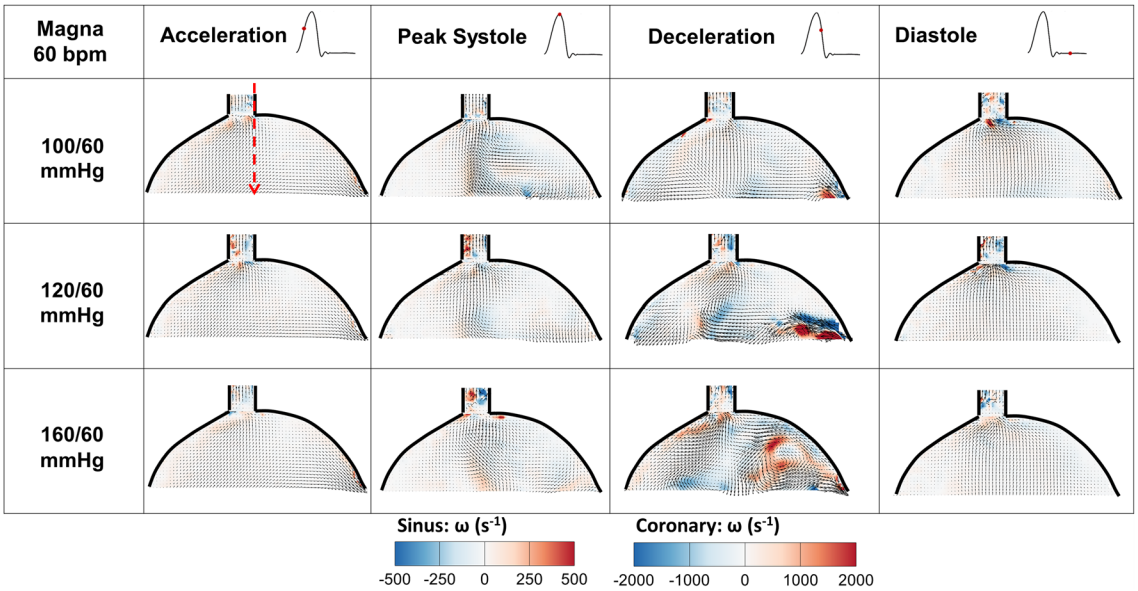

Fig. 4 Velocity vectors and vorticity contours in the sinus with increasing SBP in the presence of Magna. The dashed red arrow represents the location of the leaflet tip

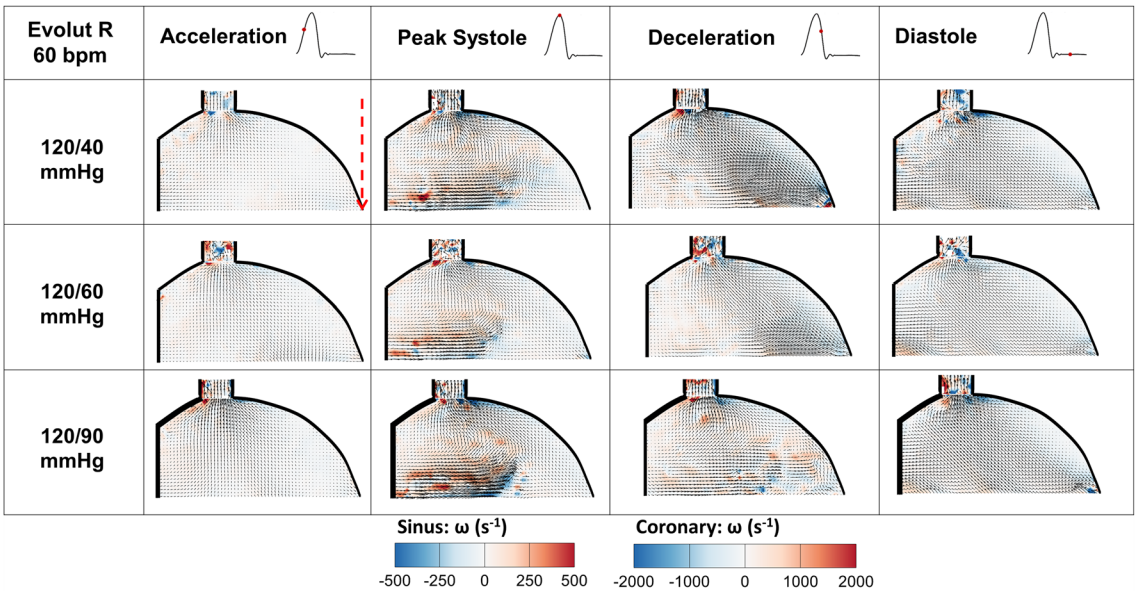

Fig. 5 Velocity vectors and vorticity contours in the sinus with increasing DBP in the presence of Evolut R. The dashed red arrow represents the location of the leaflet tip

to 0.0714 m/s as DBP increased from 40 to 90 mmHg. During deceleration, the average sinus velocity decreased from 0.187 to 0.0608 m/s. A decrease in vorticity distribution and magnitude was noted during deceleration, whereas an unchanged pattern was noted during peak systole.

Shear Stress Distribution Nearby the Leaflet

Figure 8 shows the probability density function (PDF) in semi-log scale of the stress distribution near the leaflet under the different pressure conditions in the presence of the 3 valves. Generally, the distribution of shear stress was

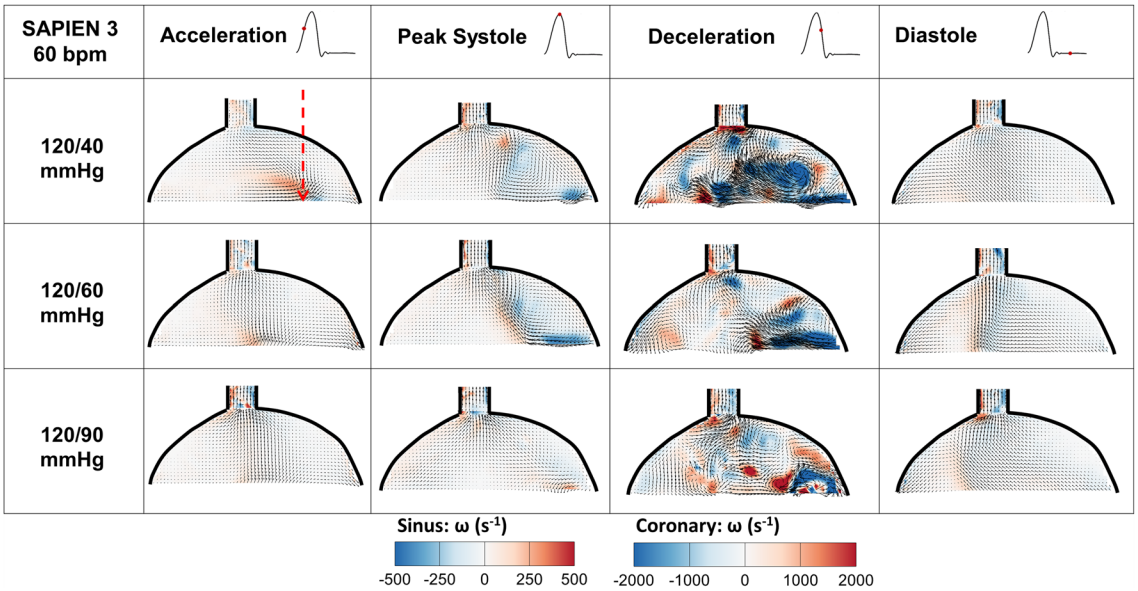

Fig. 6 Velocity vectors and vorticity contours in the sinus with increasing DBP in the presence of SAPIEN 3. The dashed red arrow represents the location of the leaflet tip

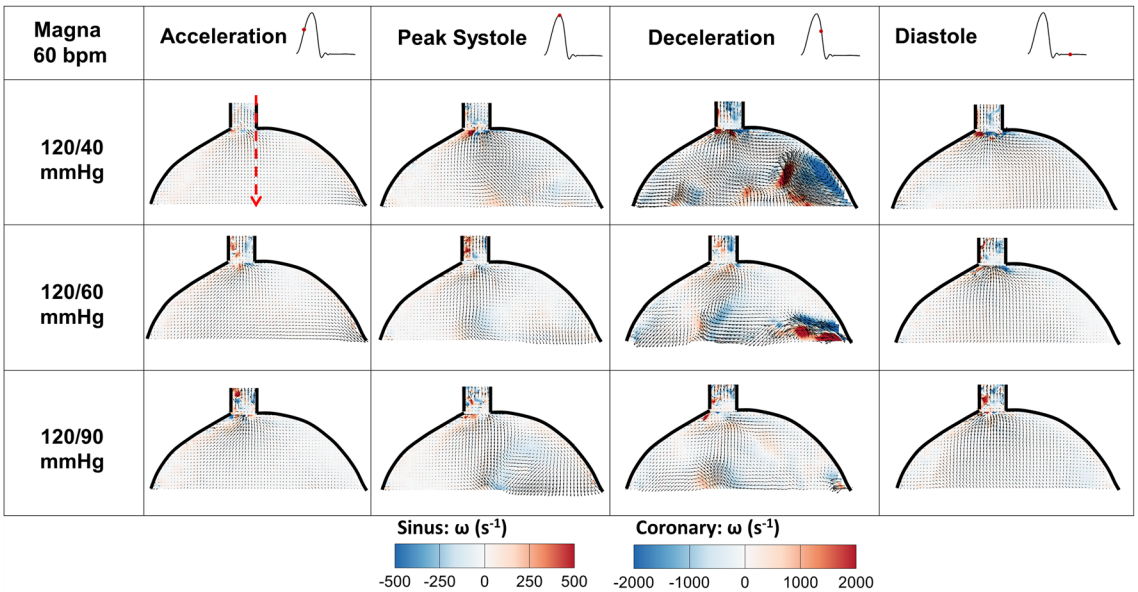

Fig. 7 Velocity vectors and vorticity contours in the sinus with increasing DBP in the presence of Magna. The dashed red arrow represents the location of the leaflet tip

very close between the blood pressure cases, especially at the higher frequencies ($> 10^{-1}$). The main differences were found in the lower frequencies (less occurrences), that led to different tails. Additionally, the results show that generally, the highest SBP and DBP led to the largest distribution and range of viscous shear stress near the leaflets' surface.

Evolut R: SBP of 160 mmHg and DBP of 90 mmHg led to the most spread-out and higher range of viscous shear stress in the region along the leaflet going from − 3.7 to 3.6 Pa and − 2.8 Pa to 3.8 Pa, respectively. The lowest SBP, 100 mmHg, showed almost the smallest range of shear stress going from − 2.2 to 2.6 Pa.

SAPIEN 3: The highest DBP (90 mmHg) led to the highest range of shear stress approximately going from − 2.0 to 2.5 Pa. The lowest range was obtained with the lowest SBP of 100 mmHg going from − 1.4 to 2.3 Pa.

Magna: The highest DBP of 90 mmHg led to the largest range of shear stress going from − 5.1 to 5.7 Pa, followed by

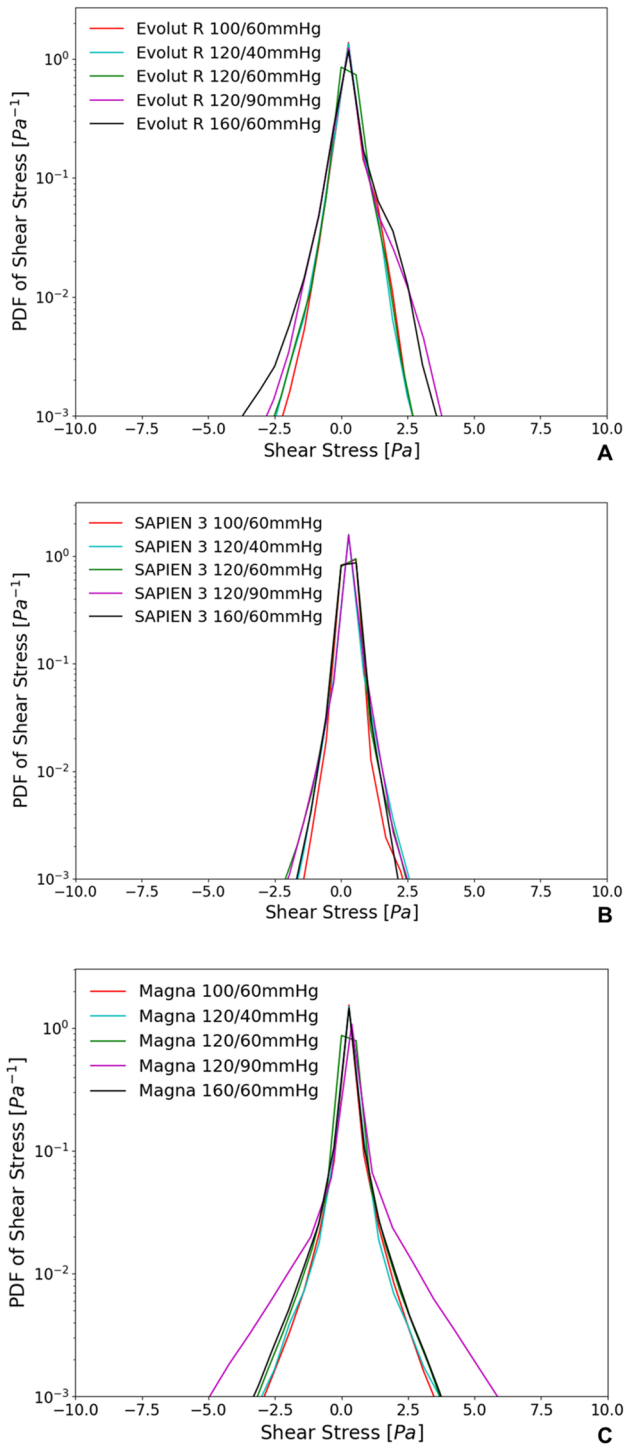

Fig. 8 Probability density function (PDF) distribution of the shear stress in the sinus in a region along the leaflet in the presence of **A** Evolut R, **B** SAPIEN 3, and **C** Magna under different pressure conditions

the highest SBP case with shear stresses going from − 3.3 to 3.7 Pa. The smallest range of shear stress was obtained with 100/60 mmHg going from − 2.9 to 3.7 Pa.

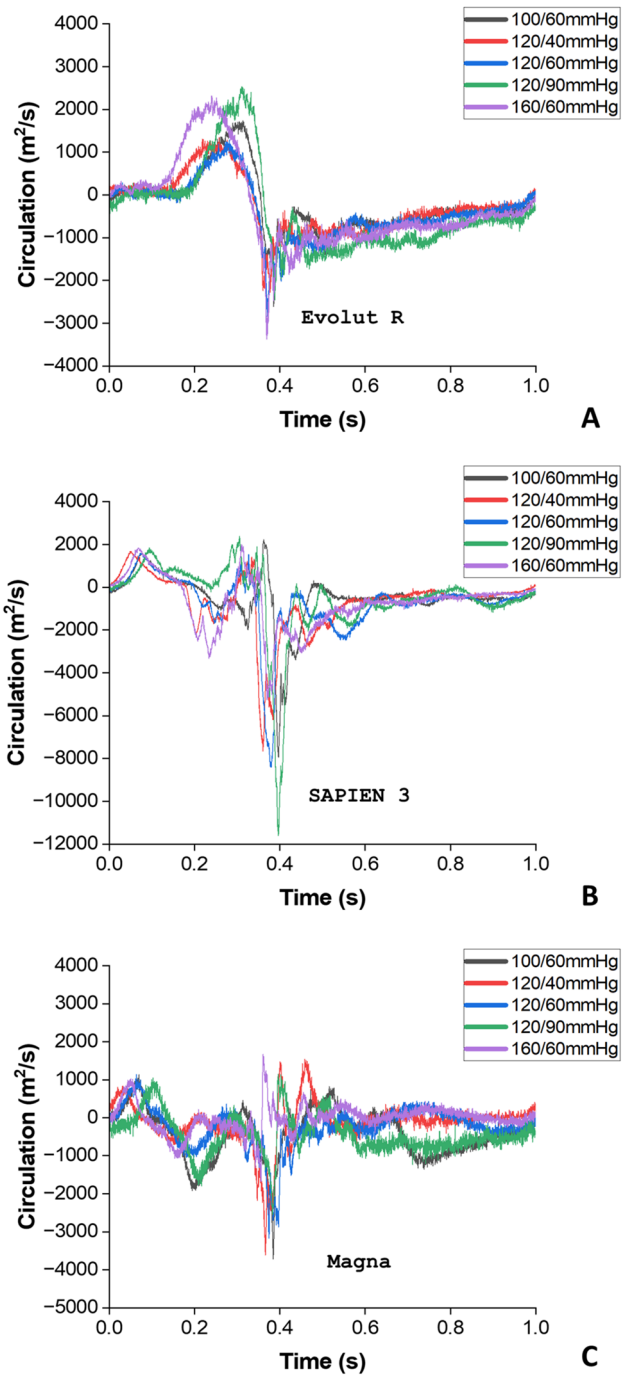

Fig. 9 Circulation plot versus time in the sinus in the presence of **A** Evolut R, **B** SAPIEN 3, and **C** Magna under different pressure conditions

Circulation (Γ) in the Sinus

The circulation (Γ) in the sinus as a function of the cardiac cycle time was plotted in Fig. 9 for all the valve and blood pressure cases. Positive circulation is counterclockwise (CCW) and negative circulation is clockwise (CW).

Evolut R: During systole for all blood pressures, Γ was mostly positive and as the valve closed, Γ became negative with values ranging from – 1000 to 0. The largest SBP and DBP led to the largest area under the curve during systole, whereas the change was minimal during diastole.

SAPIEN 3: More fluctuating Γ patterns were found with positive and negative peaks occurring during systole mainly. The largest SBP and DBP induced the largest fluctuations in Γ magnitudes.

Magna: Like the SAPIEN 3, Γ was fluctuating between positive and negative instead of keeping a uniform profile. The largest SBP and DBP led to the largest fluctuations seen throughout the cardiac cycle.

Discussion

This study aimed to assess the effect of changing SBP and DBP on valve and sinus hemodynamics with 3 different valve types. Blood flow plays an important role in hemostasis and subsequently leaflet calcification potential. Non-physiological alterations in flow can trigger abnormal cell responses in the aortic valve leaflets [31]. The cause of CAVD is not yet fully understood; however, several studies highlighted that valve calcification is an active process that involves multiple factors such as endothelial dysfunction, inflammatory responses, mineralization, oxidative stresses, and abnormal flow dynamics [2, 25, 32]. Hypertension is also one of the common risk factors of CAVD [33]. Over 60% of hypertensive patients develop CAVD [34]. Whether or not the relationship between hypertension and CAVD is founded on changes in sinus hemodynamics remains unanswered.

To understand the flow dynamics in the coronary sinus under different conditions of blood pressure, it is important to understand how SBP and DBP affect coronary flow, which may lead to alterations on the flow inside the sinus. DBP has an important role in coronary perfusion. Generally, low DBP has been associated with myocardial ischemia [35, 36] and is a key factor in coronary perfusion pressure. SBP occurs due to the stretch that large arteries undergo to accommodate the systolic ejection volume. As SBP increases, the metabolic demands of the myocardium increase, leading to a potential increase in the coronary flow [37].

Increasing SBP or DBP did not change the flow structures' (the main sinus vortex during systole as the leaflets are fully open or the secondary vortices) presence in the sinus. However, it changed the resulting velocity and vorticity magnitudes. With increasing SBP, the average velocity in the sinus and the vorticity magnitudes also increased with more expanded regions, specifically noted at peak systole and deceleration. With increasing DBP, the average velocity in the sinus generally increased only the increase was not as notable as that achieved with the increasing SBP. Vorticity kept an almost unchanged pattern. These features were uniform across all the valve types. A potential explanation of this increase in velocity and vorticity in the sinus may be related to the effect of hypertension on the effective orifice area of the valve. In a previous study by our lab, we showed that as blood pressures increase, EOA also increases [22]. Kadem et al. also showed that an increase in aortic pressure leads to aortic root expansion and stretching of the free edge of the valve leaflet, which results in an increase in the valve orifice area [38]. An increase in the aortic valve area changes the point on the leaflets where shear layers separate prior to entering inside the sinus. This allows the vortex to propagate inside the sinus at a closer distance without losing as much momentum. Typically, more elevated velocities in the sinus are desired as flow stasis is associated with CAVD [25]. However, this study shows that the mechanism of CAVD and blood pressure association needs to still be investigated further. Because of the velocity changes, and as vorticity is the curl of the velocity, the higher these changes are the higher the subsequent vorticity changes. These changes were also reflected in the circulation (Γ) results (Eq. 3) that showed that the largest SBP and DBP led to the largest fluctuations and areas under the curve seen throughout the cardiac cycle. With the Evolut R, a CCW vortex was mostly prevalent in all blood pressure cases whereas with the SAPIEN 3 and the Magna, the Γ fluctuations show more interaction and change of direction between the vortices. The durability of Magna valves is longer than THVs in general despite the fluctuations in Γ waveforms. However, the magnitudes of these fluctuations were smaller compared to the SAPIEN 3's.

An increase in SBP and DBP led to an increase in the range of shear stress in the nearby region along the leaflet at the smaller frequencies, however, the curves were relatively close to each other at the more elevated frequencies of occurrence. Shear stress is an important metric that dictates the response of the cells to the flow. It is a factor that has been used in literature in connection with valve leaflet calcification and considered one of the regulators of the CAVD process [2, 13, 25, 39]. Shear stress depends on how the velocity varies with displacement (Eq. 2), and therefore the intensity of the velocity gradient (explained in the velocity and vorticity section above) dictates the variation in shear stress. In previous sinus studies, higher shear stress values near the leaflets were desirable [12–16] only the threshold at which shear stress becomes harmful and incites abnormal cell responses within the leaflets is not well known. Systolic and diastolic hypertension was found to be associated with faster aortic valve calcification progression [8, 40].

The study had a few limitations. First, our aortic root chamber used is rigid and not patient specific. However, in our system, a compliance chamber is placed downstream of the aortic valve to mimic arterial distensibility. Moreover,

our setup allows us to study the sole effect of blood pressure variations under highly controlled conditions. Second, our aortic root does not include material to represent native leaflets that would be present after TAVR. The design of our aortic chamber is detailed in Hatoum et al. [16]. Third, our in-vitro setup is not an appropriate system to represent coronary circulation, however, it can accurately emulate epicardial coronary flow. Lastly, PIV can only capture the two velocity components (V_x and V_y) in a plane of the flow section and therefore it is not a suitable approach for an accurate estimation of the wall shear stress in a complex 3D environment.

In summary, this study assessed the impact of varying systolic and diastolic blood pressures on the hemodynamics in the sinus in the presence of Evolut R, SAPIEN 3, and Magna valves. Elevated blood pressures were associated with higher velocity, vorticity, and shear stress near the leaflets which may initiate or incite pro-calcific changes in the prosthetic leaflets leading to bioprosthetic valve degeneration. More studies are needed to characterize the full 3D environment, determine a threshold for velocity and shear stress, and calculate the resulting wall shear stress on the leaflets to understand further how blood pressure may influence CAVD progression.

Supplementary Information The online version contains supplementary material available at https://doi.org/10.1007/s10439-023-03426-4.

Acknowledgements This research was funded by the National Science Foundation award number 2301649. Brennan Vogl was partially funded by the DeVlieg foundation and the Blue Cross Blue Shield of Michigan Foundation award. Dr. Lindman is supported by grants from the National Institutes of Health (R01HL164526, R01AG073633).

Funding This research was funded by the National Science Foundation award number 2301649. Brennan Vogl was partially funded by the DeVlieg foundation and the Blue Cross Blue Shield of Michigan Foundation award. Dr. Lindman is supported by grants from the National Institutes of Health (R01HL164526, R01AG073633). Dr. Lindman has consulted for and received investigator-initiated grant funding from Edwards Lifesciences.

Declarations

Competing Interests The authors do not report any relevant conflict of interest.

References

1. Willner, N., et al. Aortic stenosis progression: a systematic review and meta-analysis. *Cardiovasc. Imaging*. 16(3):314–328, 2023.
2. Vogl, B. J., et al. Impact of calcific aortic valve disease on valve mechanics. *Biomech. Model. Mechanobiol.* 21:1–23, 2022.
3. Lindman, B. R., and W. D. Merryman. Unloading the stenotic path to identifying medical therapy for calcific aortic valve disease: barriers and opportunities. *Circulation*. 143(15):1455–1457, 2021.
4. Kostyunin, A., et al. Degeneration of bioprosthetic heart valves. Update, 2020. *J. Am. Heart Assoc.* 2020. https://doi.org/10.1161/JAHA.120.018506.
5. Zhang, B., et al. Association of bioprosthetic aortic valve leaflet calcification on hemodynamic and clinical outcomes. *J. Am. Coll. Cardiol.* 76(15):1737–1748, 2020.
6. Kostyunin, A. E., et al. Degeneration of bioprosthetic heart valves: update 2020. *J. Am. Heart Assoc.* 9(19):e018506, 2020.
7. Mancusi, C., et al. Management of patients with combined arterial hypertension and aortic valve stenosis: a consensus document from the Council on Hypertension and Council on Valvular Heart Disease of the European Society of Cardiology, the European Association of Cardiovascular Imaging (EACVI), and the European Association of Percutaneous Cardiovascular Interventions (EAPCI). *Eur. Heart J.* 7(3):242–250, 2021.
8. Iwata, S., et al. Higher ambulatory blood pressure is associated with aortic valve calcification in the elderly: a population-based study. *Hypertension*. 61(1):55–60, 2013.
9. Tastet, L., et al. Systolic hypertension and progression of aortic valve calcification in patients with aortic stenosis: results from the PROGRESSA study. *Eur. Heart J.* 18(1):70–78, 2017.
10. Rieck, Å. E., et al. Hypertension in aortic stenosis: implications for left ventricular structure and cardiovascular events. *Hypertension*. 60(1):90–97, 2012.
11. Antonini-Canterin, F., et al. Symptomatic aortic stenosis: does systemic hypertension play an additional role? *Hypertension*. 41(6):1268–1272, 2003.
12. Hatoum, H., and L. P. Dasi. Sinus hemodynamics in representative stenotic native bicuspid and tricuspid aortic valves: an in-vitro study. *Fluids*. 3(3):56, 2018.
13. Hatoum, H., et al. Impact of patient-specific morphologies on sinus flow stasis in transcatheter aortic valve replacement: an in vitro study. *J. Thorac. Cardiovasc. Surg.* 157(2):540–549, 2019.
14. Hatoum, H., et al. Implantation depth and rotational orientation effect on valve-in-valve hemodynamics and sinus flow. *Ann. Thorac. Surg.* 106(1):70–78, 2018.
15. Hatoum, H., et al. Sinus hemodynamics variation with tilted transcatheter aortic valve deployments. *Ann. Biomed. Eng.* 47:75–84, 2019.
16. Hatoum, H., et al. Aortic sinus flow stasis likely in valve-in-valve transcatheter aortic valve implantation. *J. Thorac. Cardiovasc. Surg.* 154(1):32-43.e1, 2017.
17. Hatoum, H., et al. An in vitro evaluation of turbulence after transcatheter aortic valve implantation. *J. Thorac. Cardiovasc. Surg.* 156(5):1837–1848, 2018.
18. Vogl, B. J., et al. Flow dynamics in the sinus and downstream of third and fourth generation balloon expandable transcatheter aortic valves. *J. Mech. Behav. Biomed. Mater.* 127:105092, 2022.
19. Gotzmann, M., et al. Hemodynamic results and changes in myocardial function after transcatheter aortic valve implantation. *Am. Heart J.* 159(5):926–932, 2010.
20. Lindman, B. R., et al. Blood pressure and arterial load after transcatheter aortic valve replacement for aortic stenosis. *Circulation*. 10(7):e006308, 2017.
21. Lindman, B. R., et al. Lower blood pressure after transcatheter or surgical aortic valve replacement is associated with increased mortality. *J. Am. Heart Assoc.* 8(21):e014020, 2019.
22. Vogl, B. J., et al. Impact of blood pressure on coronary perfusion and valvular hemodynamics after aortic valve replacement. *Catheter. Cardiovasc. Interv.* 99(4):1214–1224, 2022.
23. Moore, B., and L. P. Dasi. Spatiotemporal complexity of the aortic sinus vortex. *Exp. Fluids*. 55:1–12, 2014.
24. Thubrikar, M., L. P. Bosher, and S. P. Nolan. The mechanism of opening of the aortic valve. *J. Thorac. Cardiovasc. Surg.* 77(6):863–870, 1979.

25. Hatoum, H., and L. P. Dasi. Spatiotemporal complexity of the aortic sinus vortex as a function of leaflet calcification. *Ann. Biomed. Eng*. 47:1116–1128, 2019.
26. David, T. E., and J. Ivanov. Is degenerative calcification of the native aortic valve similar to calcification of bioprosthetic heart valves? *J. Thorac. Cardiovasc. Surg*. 126(4):939–941, 2003.
27. Sun, L., S. Chandra, and P. Sucosky. Ex vivo evidence for the contribution of hemodynamic shear stress abnormalities to the early pathogenesis of calcific bicuspid aortic valve disease. *PLoS ONE*. 7(10):e48843, 2012.
28. Jhun, C.-S., et al. Dynamics of blood flows in aortic stenosis: mild, moderate, and severe. *ASAIO J. (1992)*. 67(6):666, 2021.
29. Vogl, B. J., et al. A Preliminary study on the usage of a data-driven probabilistic approach to predict valve performance under different physiological conditions. *Ann. Biomed. Eng*. 50(8):941–950, 2022.
30. Hughes-Hallett, D., A. M. Gleason, and W. G. McCallum. Calculus: Single and Multivariable. Nashville: Wiley, 2020.
31. Hoehn, D., L. Sun, and P. Sucosky. Role of pathologic shear stress alterations in aortic valve endothelial activation. *Cardiovasc. Eng. Technol*. 1:165–178, 2010.
32. Sathyamurthy, I., and S. Alex. Calcific aortic valve disease: is it another face of atherosclerosis? *Indian Heart J*. 67(5):503–506, 2015.
33. Kadel, S. Computational assessment of aortic valve function and mechanics under hypertension. Wright State University, 2020.
34. Cameli, M., et al. Identification of cardiac organ damage in arterial hypertension: insights by echocardiography for a comprehensive assessment. *J. Hypertens*. 38(4):588–598, 2020.
35. Khan, N. A., et al. Effect of lowering diastolic pressure in patients with and without cardiovascular disease: analysis of the SPRINT (Systolic Blood Pressure Intervention Trial). *Hypertension*. 71(5):840–847, 2018.
36. Hsieh, M.-J., et al. Risk stratification by coronary perfusion pressure in left ventricular systolic dysfunction patients undergoing revascularization: a propensity score matching analysis. *Front. Cardiovasc. Med*. 2022. https://doi.org/10.3389/fcvm.2022.860346.
37. Rabkin, S. W. Considerations in understanding the coronary blood flow- left ventricular mass relationship in patients with hypertension. *Curr. Cardiol. Rev*. 13(1):75–83, 2017.
38. Kadem, L., et al. Impact of systemic hypertension on the assessment of aortic stenosis. *Heart*. 91(3):354–361, 2005.
39. Sucosky, P., et al. Altered shear stress stimulates upregulation of endothelial VCAM-1 and ICAM-1 in a BMP-4–and TGF-β1–dependent pathway. *Arterioscler. Thromb. Vasc. Biol*. 29(2):254–260, 2009.
40. Tastet, L., et al. Systolic hypertension and progression of aortic valve calcification in patients with aortic stenosis: results from the PROGRESSA study. *Eur. Heart J. Cardiovasc. Imaging*. 18(1):70–78, 2017.